Technical Report

Title:	*Diffusion of $^{125}I^-$ in Limestone and Red Shale Samples from DGR-2*
Document ID:	**TR-07-22**
Author:	**L. R. Van Loon, Paul Scherrer Institute**
Revision:	**1**
Date:	**June 18, 2010**

DGR Site Characterization Document
Intera Engineering Project 06-219

Intera Engineering DGR Site Characterization Document		
Title:	Diffusion of ^{125}I$^-$ in Limestone and Red Shale Samples from DGR-2.	
Document ID:	TR-07-22	
Revision Number:	1	Date: June 18, 2010
Author:	L. R. Van Loon, Paul Scherrer Institute, Switzerland	
Technical Review:	Kenneth Raven, Tom Al (University of New Brunswick), Dylan Luhowy, Jennifer McKelvie (NWMO)	
QA Review:	John Avis	
Approved by:	Kenneth Raven	

Document Revision History		
Revision	Effective Date	Description of Changes
0	November 18, 2009	Initial release
1	June 18, 2010	Minor revisions to address NWMO editorial comments of June 15, 2010. Updating of references.

TABLE OF CONTENTS

LIST OF FIGURES

LIST OF TABLES

LIST OF APPENDICES

APPENDIX A   Experimental Data

INTERA

1   Introduction

Intera Engineering Ltd. has been contracted by the Nuclear Waste Management Organization (NWMO) on behalf of Ontario Power Generation to implement the Geoscientific Site Characterization Plan (GSCP) for the Bruce nuclear site located near Tiverton, Ontario. The purpose of this site characterization work is to assess the suitability of the Bruce site to construct a Deep Geologic Repository (DGR) to store low- and intermediate-level radioactive waste. The GSCP is described by Intera Engineering Ltd. (2006, 2008).

This Technical Report (TR) presents the results from laboratory measurements of diffusion properties of shale and limestone samples from deep borehole DGR-2, Bruce site, Ontario. Diffusion testing was completed by the Waste Management Laboratory, Diffusion Processes Group, Paul Scherrer Institute, Villigen, Switzerland under contract to Intera Engineering Ltd.

The Paul Scherrer Institute, Switzerland (PSI) performed through-diffusion measurements with [125]I⁻ on two different samples originating from borehole DGR-2, Bruce nuclear site in southern Ontario, Canada. The measurements had to be performed in anoxic conditions in an inert gas glove box. Because the pore waters to be used in the experiments were highly saline, the existing PSI diffusion cells made from 316L stainless steel (Van Loon and Soler, 2004) had to be modified. Also alternatives for the stainless steel filters had to be evaluated. Moreover, the different behaviour of the samples when in contact with water forced the use of an alternative method for sample preparation, and to adapt the experimental protocol used for through-diffusion measurements on Opalinus Clay samples from the Swiss Waste Management Program (Van Loon et al., 2003a; Van Loon et al., 2003b; Glaus et al., 2008). Data for the two types of Paleozoic rock samples tested here are also available in Vilks and Miller (2007) and Cavé et al. (2009).

Work described in this Technical Report was completed in accordance with Test Plan TP-06-12 – Measurement of Diffusion Properties by X-Ray Radiography (Intera Engineering Ltd., 2007), with the exception that testing was limited to use of [125]I⁻ tracers. This Technical Report was prepared following the general requirements of the Intera DGR Project Quality Plan (Intera Engineering Ltd., 2009).

2   Materials and Methods

2.1   Samples

The samples used were Cobourg Formation argillaceous limestone (DRG2-675.48) and Queenston Formation red shale (DRG2-466.38). The samples (Figure 1) were provided to PSI by Intera Engineering Ltd.

Figure 1   Samples from the deep borehole DGR2 used in the through-diffusion measurements (limestone: left; red shale: right)

Slices of ca. 8-10 mm thickness were prepared by dry cutting (Figure 2) using a diamond wire saw (Well). After cutting, the samples were embedded in an epoxy resin (Epofix, Struers GmbH). After hardening of the resin, the cylinder was placed on a lathe and the resin at the front ends were removed (Figure 3).

Figure 2   Preparation of the 8-10 mm slices by dry cutting with a diamond wire saw

Figure 3   Red shale (left) and limestone (right) samples embedded in epoxy resin

2.2   Synthetic Pore Waters

Synthetic pore waters (SPW) were prepared by dissolving Na-, K-, Ca- and Mg-salts in Milli-Q water. The composition of the synthetic pore waters (SPW) used is given in Table 1.

Table 1   Composition of the synthetic porewaters (SPW) used in the diffusion experiments

Parameter	Red shale SPW (mol/L)	Limestone SPW (mol/L)
Na	2.40	2.00
K	0.50	0.45
Ca	1.201	0.485
Mg	0.25	0.20
Cl	5.80	3.81
SO$_4$	0.001	0.005

2.3   Diffusion Cells

A new diffusion cell was designed that allowed us to use samples with a diameter of 76 mm and a thickness between 5 and 20 mm. Because of the high salinity of the porewater (see Table 1) the diffusion cells were made of Ertolyte®, an unreinforced polyester based on polyethylene terephthalate. Porous polyethylene filters (diameter =76 mm, thickness L=1.5 mm, porosity ε_F=0.45) were used to confine the samples (Figure 4).
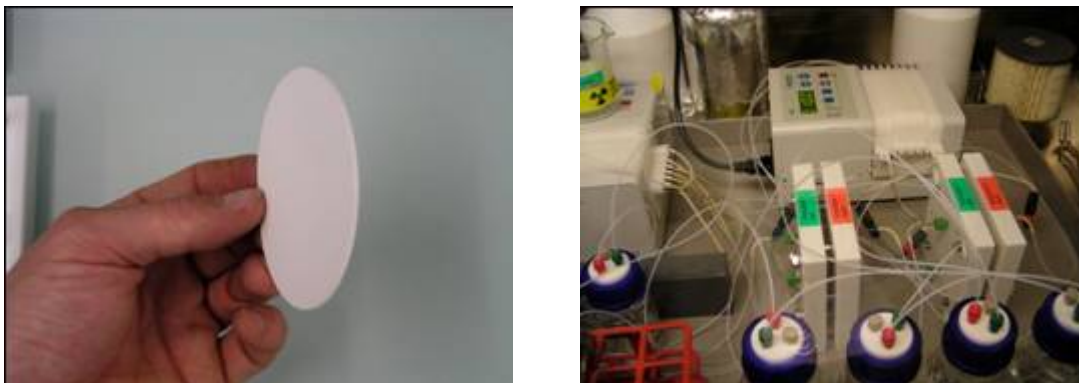
Figure 4   Polyethylene filter (left) and diffusion cells (right) used in the experiments

2.4   Diffusion Experiments

The samples (embedded in epoxy resin) were sandwiched between two porous filters and mounted in the diffusion cells with the bedding plane perpendicular to the direction of diffusion. The filters were presaturated with water under vacuum. The cells were connected to 2 reservoirs containing synthetic porewater (SPW) and circulated using a peristaltic pump (IPC, Ismatec, Idex Corporation, USA). After a resaturation period of 1 month, the reservoirs were replaced. A reservoir containing 500 cm^3 SPW spiked with ^{125}I$^-$ was connected to one side of the diffusion cell. The activity concentration in this reservoir was ca. 5000 Bq/mL. A low concentration reservoir containing 20 cm^3 SPW was connected to the other side of the cell. The solution at the low concentration side was regularly replaced after a time interval Δt (typical 2-3 days) to keep the concentration of the tracer in this compartment as low as possible, i.e. <1% of the concentration in the high-concentration compartment. Activities in the samples were measured with a γ-counter (Cobra, Canberra-Packard) and were corrected for radioactive decay.

The experiments were performed under N$_2$ in an inert gas glove box (MBraun, München, Germany; see Fig. 5) under anoxic conditions (O$_2$<2ppm). The temperature in the glove box was 24±1 ^{o}C.

Figure 5   Inert gas glove box in the controlled area of the hotlab facility at PSI

2.5   Data Processing

After a time t_i, the low activity container, having a volume V_{low}, is replaced by the same volume of solution, but containing no radiotracer. A given volume (V_{sample}) of this sampled solution is used for the activity measurements as described above (counting time is T) and gives a count rate, $N_T^{t_i}$ [cpm]. The background is measured under similar conditions resulting in a count rate, $N_o^{t_i}$ [cpm]. From these two measurements, a net count rate, $N_s^{t_i}$ [cpm], is calculated as:

$$N_s^{t_i} = N_T^{t_i} - N_o^{t_i} \tag{1}$$

The total amount of tracer [cpm] diffused through the sample during a time interval $\Delta t_i = t_i - t_{i-1}$ is calculated by:

$$N_{dif}^{\Delta t_i} = \frac{N_s^{t_i}}{V_{sample}} \cdot V_{low} + \frac{N_s^{t_i}}{V_{sample}} \cdot V_{dead} - \frac{N_s^{t_{i-1}}}{V_{sample}} \cdot V_{dead} \tag{2}$$

where V_{dead} is the volume that is not replaced when changing the solution in the low concentration reservoir and represents the dead volume, i.e. the volume of the tubing, the grooves in the end plates and the filter pore space. The negative term in Eqn. 2 represents the correction for the activity left in this dead volume when replacing the solution in the container. At time t_o, the count rate, $N_s^{t_o}$, is zero. So for $i=1$, i.e. the first sampling, the total amount of tracer [cpm] diffused is:

$$N_{dif}^{\Delta t_1} = \frac{N_s^{t_1}}{V_{sample}} \cdot V_{low} + \frac{N_s^{t_1}}{V_{sample}} \cdot V_{dead} \tag{3}$$

The activity A [Bq] diffused through the rock during a time Δt_i is now given by:

$$A_{dif}^{\Delta t_i} = \frac{N_{dif}^{\Delta t_i}}{60 \cdot f}$$

(4)

where f [cps·Bq^{-1}] is the counting efficiency (for ^{125}I, the counting efficiency is 70%). The average flux during Δt_i, $J_L^{t_i}$ [Bq·m^{-2}·s^{-1}], is calculated by:

$$J_L^{t_i} = \frac{A_{dif}^{\Delta t_i}}{S \cdot \Delta t_i}$$

(5)

where S represents the cross section area [m^2]. The accumulated activity A diffused through the rock sample after diffusion time t_n is:

$$A_{dif}^{t_n} = \sum_{i=1}^{n} A_{dif}^{\Delta t_i}$$

(6)

The uncertainty on the values of the fluxes and on the accumulated diffused activities in the through-diffusion measurements results from the uncertainty on the parameters involved to calculate these values. A detailed description of the procedure to calculate the uncertainty is given in Van Loon and Soler (2004).

3   Results and Discussion

3.1   Theoretical Background of One-Dimensional Through Diffusion

For a one-dimensional diffusion process through a plane with thickness L the flux, J, is given by Fick's first law:

$$J = -D_e \cdot \frac{\partial C}{\partial x}$$

(7)

where D_e (m^2.s^{-1}) is the effective diffusion coefficient and C the concentration of the tracer in the liquid phase and X is the diffusion distance. If the concentration within the system is changing, Fick's second law applies:

$$\frac{\partial C}{\partial t} = D_a \cdot \frac{\partial^2 C}{\partial x^2}$$

(8)

where D_a (m^2.s^{-1}) is the apparent diffusion coefficient, defined as:

$$D_a = \frac{D_e}{\alpha}$$

(9)

The rock capacity factor, α, is given by:

$$\alpha = \varepsilon + \rho \cdot K_d$$

(10)

where K_d = the equilibrium distribution coefficient (m^3·kg^{-1})

ρ = the dry bulk density of the rock (kg·m^{-3})

ε = diffusion accessible porosity (-)

For non-sorbing tracers ($K_d = 0$), the rock capacity factor equals the transport porosity. For $K_d > 0$, the diffusion accessible porosity can be deduced from the rock capacity factor by:

$$\varepsilon = \alpha - \rho \cdot K_d \tag{11}$$

This, however, requires knowledge of the K_d value. The main problem hereby is the fact that K_d values are in general measured on powdered samples suspended in a relatively large volume of solution. Whether it is justified to use these values for intact samples is questionable. So far, the uncertainty on porosity values derived from diffusion studies with sorbing tracers is relatively large.

The effective diffusion coefficient, D_e, is related to the diffusion coefficient in free water D_w (m^2.s^{-1}) by:

$$D_e = \frac{\varepsilon \cdot \delta}{\tau^2} \cdot D_w \tag{12}$$

δ (-) is the constrictivity and accounts for the fact that the pore diameter varies along the pathway, and τ (-) is the tortuosity of the sample and takes account for path lengthening. The three parameters are mostly lumped together in a geometric factor G (-):

$$G = \frac{\varepsilon \cdot \delta}{\tau^2} \tag{13}$$

Figure 6 is a schematic representation of one-dimensional diffusion through a homogeneous and isotropic porous medium (rock) with thickness L. The initial condition for the system is:

$$C(x,t) = 0 \; ; \; x \in [0,L], \, t = 0$$

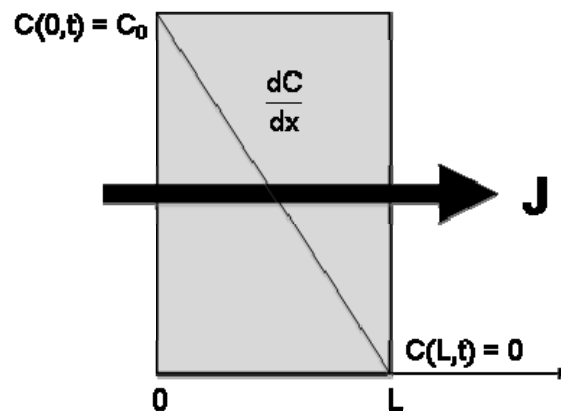meaning that the rock sample is originally free of tracer.

Figure 6   One dimensional diffusion through a homogeneous and isotropic porous medium with thickness L. The solid line represents the concentration profile of the tracer in the pore water at steady state

The boundary conditions for the system in our experimental set-up are:

$$C(0,t) = C_o = constant \; ; \; t > 0 \; and \; C(L,t) = 0 \; ; \; t > 0$$

where $C(0,t) = C_o$ (Bq·m^{-3}) is the concentration of tracer at the high-concentration side and $C(L,t)$ (Bq·m^{-3}) is the concentration of tracer at the low-concentration side (measurement cell). At steady-state the concentration gradient in the sample along the x-direction is assumed to be linear (Figure 6). The analytical solution to the through-diffusion problem is obtained by solving Eqn. (8) with the initial and boundary conditions given above and making use of the fact that the flux of the tracer at the low-concentration boundary at x=L according to Eqn. (7) is:

$$J(L,t) = -D_e \cdot \frac{\partial c}{\partial x}\bigg|_{x=L} \tag{14}$$

The analytical solution is (Crank, 1975; Jakob et al., 1999):

$$A_{dif}^t = S \cdot L \cdot C_o \cdot \left(\frac{D_e \cdot t}{L^2} - \frac{\alpha}{6} - \frac{2 \cdot \alpha}{\pi^2} \sum_{n=1}^{\infty} \frac{(-1)^n}{n^2} \cdot exp\left\{ -\frac{D_e \cdot n^2 \cdot \pi^2 \cdot t}{L^2 \cdot \alpha} \right\} \right) \tag{15}$$

Eqn. (15) gives the cumulative mass or activity of a tracer in the low-concentration reservoir as a function of time. One of the boundary conditions used to solve the differential equation specifies that the concentration of the tracer at the low-concentration boundary of the cell must be equal to zero. However, as long as $C(L,t) << C_o$, the analytical solution approximates well Eqn. (15). As time increases, the exponential term reduces towards zero and Eqn. (15) approximates:

$$A_{dif}^t = S \cdot L \cdot C_o \cdot \left(\frac{D_e \cdot t}{L^2} - \frac{\alpha}{6} \right) \tag{16}$$

Figure 7 shows data of a hypothetical through-diffusion experiment. Both the flux and the total accumulated mass are presented. Two stages can be distinguished. In a first stage the flux increases. As long as the flux increases, the diffusion process is in a transient phase. As soon as the flux reaches a constant value, the process is in steady state. In this stage, the total accumulated mass increases linearly with time. From the data acquired in the steady state phase, a diffusion coefficient (D_e) and a transport relevant porosity value (ε) can be derived. When the diffusion process is in the steady state phase, the total diffused mass thus becomes a linear function of time:

$$A_{dif}^t = a \cdot t + b \tag{17}$$

where

$$a = \frac{S \cdot C_o \cdot D_e}{L} \tag{18}$$

and

$$-b = \frac{S \cdot L \cdot C_o \cdot \alpha}{6} \tag{19}$$
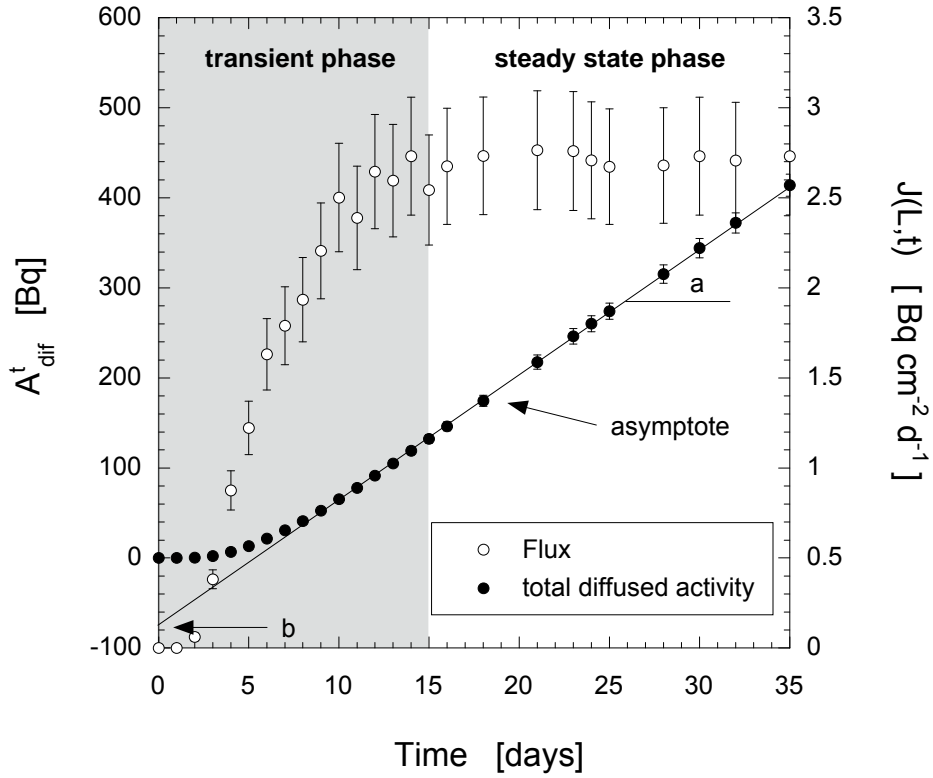
Figure 7   **Evolution of flux and total diffused mass as a function of time in a through diffusion experiment**

The straight line in Figure 7 shows this linear equation. From the slope of the line and the intercept with the y-axis, both D_e and α can be calculated:

$$D_e = \frac{a \cdot L}{S \cdot C_o} \qquad (20)$$

and

$$\alpha = -\frac{6 \cdot b}{S \cdot L \cdot C_o} \qquad (21)$$

The propagated uncertainty on D_e and ε were calculated by combining the relative errors on the individual parameters a, b, L, S and C_o:

$$u(D_e) = D_e \cdot \sqrt{(r.u.(a))^2 + (r.u.(L))^2 + (r.u.(S))^2 + (r.u.(C_o))^2} \qquad (22)$$

$$u(\alpha) = \alpha \cdot \sqrt{(r.u.(b))^2 + (r.u.(L))^2 + (r.u.(S))^2 + (r.u.(C_o))^2} \qquad (23)$$

3.2   Results for Limestone Samples (Cobourg Formation)

Figure 8 shows the results of the through-diffusion measurements performed on two samples of the limestone from the Cobourg Formation cut from sample DGR2-.675.48. The total diffused mass as a function of time is plotted.
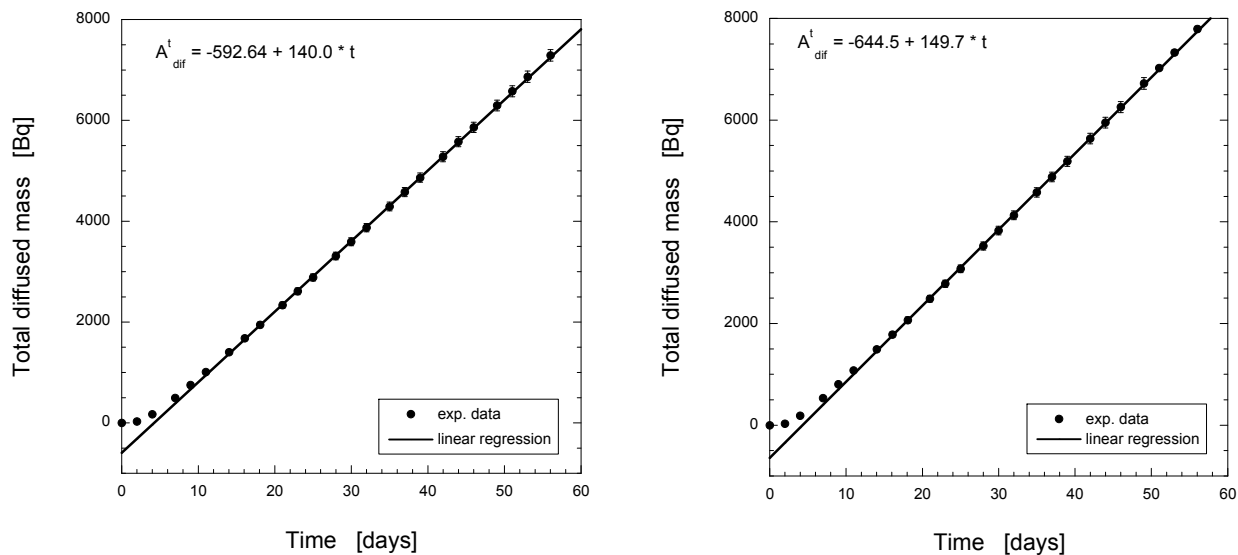
Figure 8   Total diffused mass vs time for the diffusion of ^{125}I$^-$ through 2 limestone samples from the Cobourg Formation

From the total diffused activity and using Eqn. (17), (20) and (21), a value for D_e and α can be calculated, assuming that steady state was reached after 10 days diffusion time, i.e. constant flux was reached. The parameter values derived are given in Table 2.

Table 2   Values of D_e and α for the Cobourg Formation (limestone) calculated from the total diffused activities. The slope and intercept represent the parameters a and b in Eqn. (17)

Parameter	Sample 1	Sample 2
Slope (a)	140.0	149.7
Intercept (b)	-592.6	-644.5
D_e (m^2 s^{-1})	6.74x10^{-13}	6.26x10^{-13}
α (-)	0.024	0.024

It can be assumed that ^{125}I$^-$ does not sorb on the limestone (K_d=0) so that the rock capacity factor, α, represents the diffusion accessible porosity, ε. In order to evaluate whether the diffusion accessible porosity of ^{125}I$^-$ equals the total porosity, diffusion experiments with HTO are necessary.
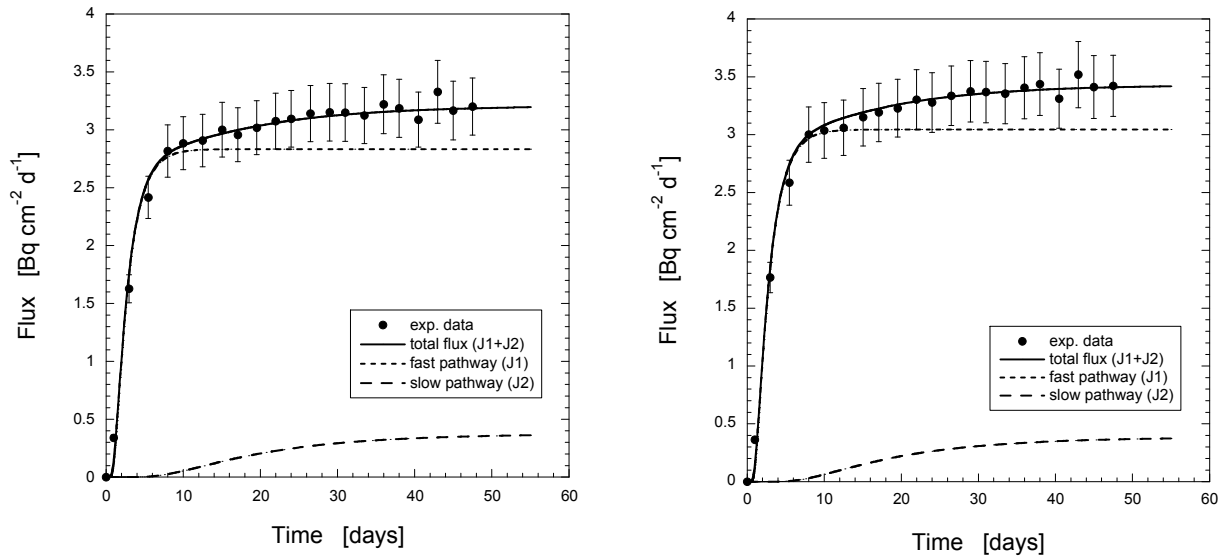
Figure 9   **Flux vs time curves for the diffusion of ^{125}I$^-$ through 2 limestone samples from the Cobourg Formation**

Figure 9 represents the flux vs. time curves for the same through-diffusion experiments. A close inspection of the curves indicates that the steady state was not reached after 10 days diffusion. The flux further increased to reach a plateau value after ca. 50 days. This is an indication for an additional diffusion pathway. The total flux can be subdivided in two fluxes:

$$J_{tot} = J_1 + J_2 = -D_{e,1} \cdot \frac{\partial C}{\partial x} - D_{e,2} \cdot \frac{\partial C}{\partial x} \qquad (24)$$

characterized by two effective diffusion coefficients, $D_{e,1}$ and $D_{e,2}$. A similar phenomenon was observed for the diffusion of HTO in Opalinus Clay (Van Loon and Jakob, 2005). A fast diffusion pathway is characterised by $D_{e,1}$ and a slow pathway by $D_{e,2}$. The flux curves in Figure 9 were calculated using COMSOL Multiphysics V3.5[1]. The results of the calculations are given in Table 3.

Table 3   **Values of D_e and α calculated for Cobourg limestone from the flux curves in Figure 9**

Parameter	Sample 1	Sample 2
$D_{e,1}$ (m^2 s^{-1})	6.10x10^{-13}	5.70x10^{-13}
α_1 (-)	0.015	0.015
$D_{e,2}$ (m^2 s^{-1})	8.00x10^{-14}	8.00x10^{-14}
α_2 (-)	0.015	0.015

---

[1] COMSOL Multiphysics is a software package which has unique features in representing multiply linked domains with complex geometry, highly coupled and nonlinear equation systems, and arbitrarily complicated boundary and initial conditions. The software is based on the finite element methods (FEM) for approximating partial differential equations (PDE) that arise in science and engineering analysis.

Also the use of the filters were taken into account. The diffusion parameters for the filters were $\alpha_F=\varepsilon_F=0.45$ and $D_F= 4.5 \times 10^{-10}$ m^2 s^{-1}. Because the effective diffusion coefficient of the filters is a factor of 10 higher than those for the samples, the contribution of the filters to the total flux is small.

As can be seen from Table 3, the slower pathway is characterised by an effective diffusion coefficient that is a factor of 7-8 smaller than that of the fast pathway. However, the largest part (85-90%) of the mass transport through the sample occurs via the fast pathway and only 10-15% via the slow pathway.

3.3 Results for Red Shale Samples (Queenston Formation)

Fig. 10 shows the total diffused mass vs time for the diffusion of ^{125}I$^-$ through the two red shale samples (Queenston Formation) cut from sample DGR2-466.38. The diffusion parameters calculated using Eqn. (17), (20) and (21) are summarised in Table 4.
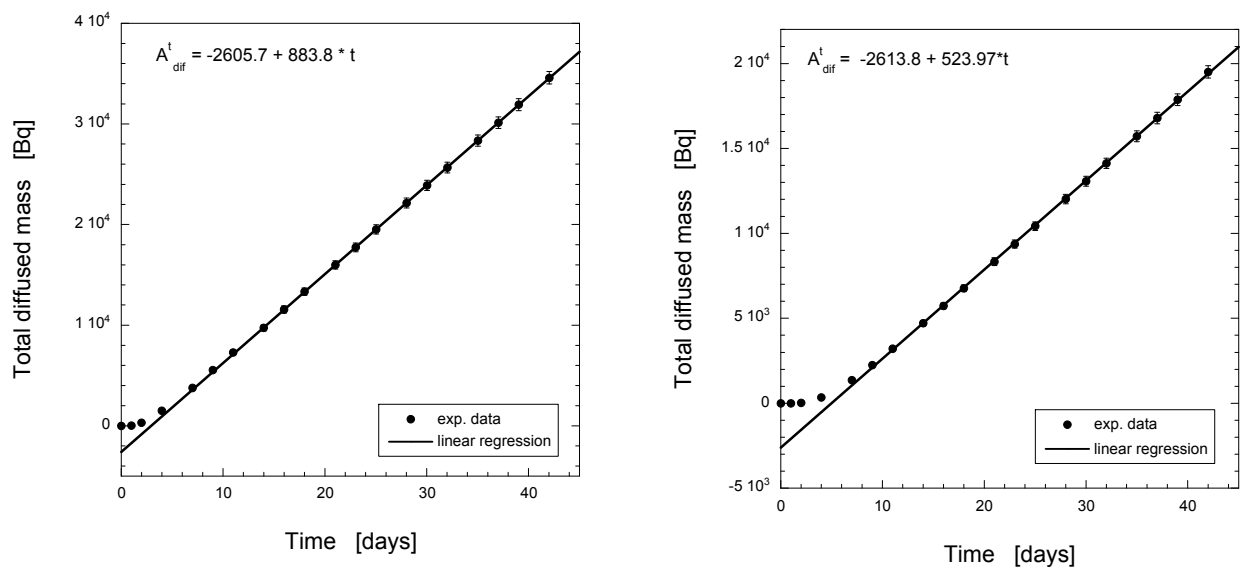
Figure 10   Total diffusion mass vs time curves for the diffusion of ^{125}I$^-$ through 2 red shale samples from the Queenston Formation

As can be seen from the Table 4, both the effective diffusion coefficient and the rock capacity factor of the red shale samples are larger than the values obtained for the limestone samples.

Table 4   Values of D_e and α for the Queenston Formation as calculated from the total diffused activities. The slope and intercept represent the parameters a and b in Eqn. (17).

Parameter	Sample 1	Sample 2
Slope (a)	883.8	524.0
Intercept (b)	-2605.7	-2613.8
D_e (m^2 s^{-1})	3.63×10^{-12}	3.05×10^{-12}
α (-)	0.134	0.096

Figure 11 shows the flux versus time curves for the diffusion of $^{125}I^-$ in the red shale samples. Unlike the limestone samples, no dual diffusion was observed for the Queenston formation. The diffusion is characterised by one single diffusion coefficient. The diffusion coefficients calculated from the flux curves are similar to those calculated from the total diffused mass. The rock capacity factor is somewhat smaller for sample 1 and identical for sample 2 (Table 5).
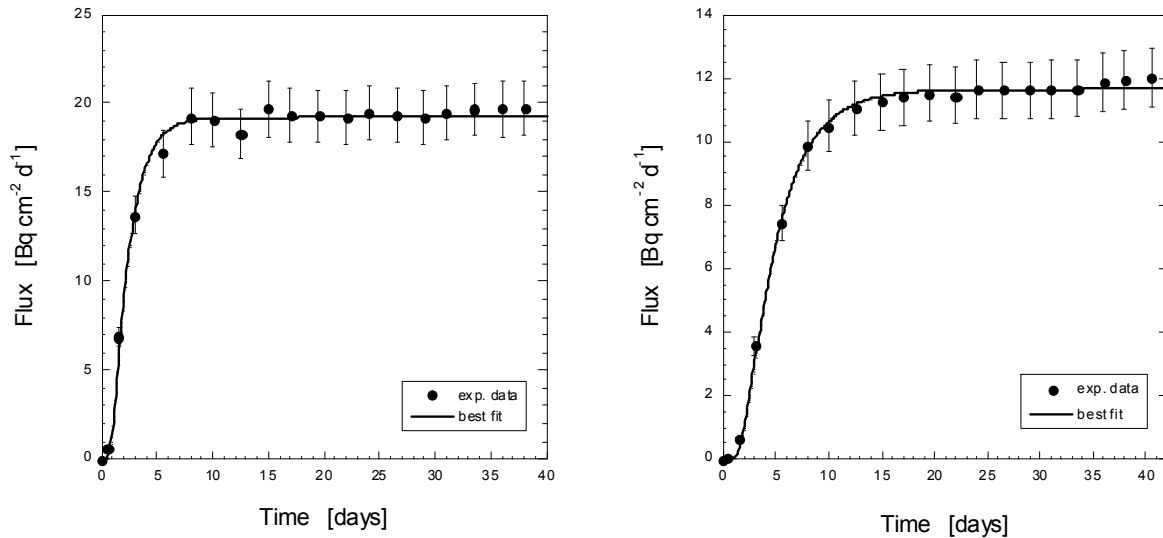
Figure 11   **Flux vs time curves for the diffusion of $^{125}I^-$ through the two red shale samples from the Queenston Formation**

Table 5   **Values of D_e and α for the red Queenston shale samples calculated from the flux curves given in Figure 11**

Parameter	Sample 1	Sample 2
D_e (m^2 s^{-1})	3.6x10^{-12}	3.0x10^{-12}
α (-)	0.11	0.10

4   Comparison with Diffusion Measurements on Other Rock Samples

4.1   Diffusion in Limestone

Diffusion of I^- and Cl^- in limestone was studied by Descostes et al. (2008) and Boving and Grathwohl (2001). Figure 12 summarizes the results in an Archie type of plot (D_e vs. diffusion accessible porosity). All results can be described very well by:

$$D_e = D_w \cdot \varepsilon^n \qquad\qquad (25)$$

where D_w is the diffusion coefficient of I^- in water (D_w=2.03x10^{-9} m^2 s^{-1}, Li and Gregory, 1974) and n=2.3.

4.2   Diffusion in Argillaceous Rocks

In the case of argillaceous rocks, only a few data could be found in the literature (Descostes et al. 2008; Van Loon et al. 2003a; Van Loon et al. 2003b; Ishidera, 2007). A similar behaviour can be observed, although the

experimental data show a larger degree of scattering. The solid line in Figure 12 represents Eqn. (25) with D_w = 2.0×10^{-9} m^2 s^{-1} (Li and Gregory, 1974) and n = 2.5.
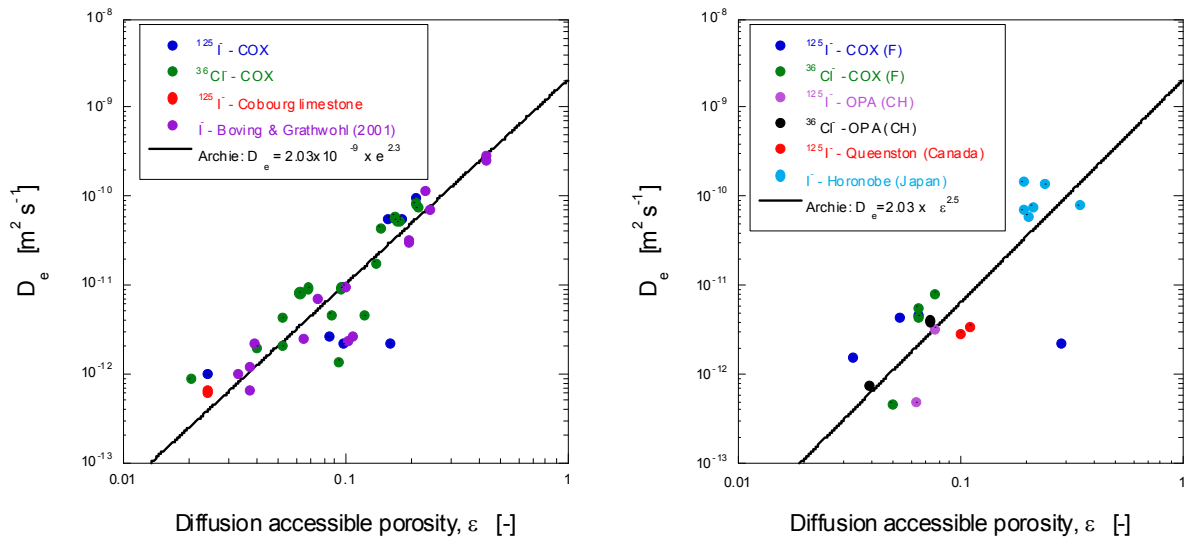
Figure 12   Comparison of diffusion data for the Cobourg Formation (left) and the Queenston Formation (right) with literature data

5   Conclusions

A new type of diffusion cell was developed to study the diffusion of radionuclides in shales and limestone under high-salinity pore water conditions. The cells were successfully tested with [125]I[-].

The diffusion coefficients (perpendicular to the bedding) and rock capacity factors measured for limestone and red shale, based on the total diffused mass vs. time curves are summarized in Table 6. The diffusion coefficients and rock capacity factors of [125]I[-] in the red shale samples are a factor of 5 higher than in the limestone samples.

Table 6   Overview of diffusion parameters calculated from the total mass vs time curves for Cobourg limestone and Queenston red shale

Rock Sample	*Sample 1*		*Sample 2*	
	D_e (m^2 s^{-1})	α (-)	D_e (m^2 s^{-1})	α ($-$)
Limestone (Cobourg Fm – DGR2-675.48)	6.74×10^{-13}	0.024	6.26×10^{-13}	0.024
Red shale (Queenston Fm – DGR2-466.38)	3.63×10^{-12}	0.134	3.05×10^{-12}	0.096

Diffusion parameters based on the flux vs. time curves are somewhat different. In the case of red shale, both the effective diffusion coefficient and the rock capacity factor are similar. In the case of limestone, two diffusion pathways could be observed: a slow one and a fast one. The majority of mass, however, diffuses through the fast pathway.

6   Data Use and Quality

Results of laboratory diffusion testing of DGR-2 core described in this Technical Report are based on testing using well established and internationally accepted through-diffusion techniques. The results are considered suitable for assessing the general range of diffusional properties of the Ordovician formations intersecting borehole DGR-2 and for benchmarking other diffusion testing recently completed by the University of New Brunswick using X-Ray radiography and through-diffusion techniques with iodide and tritium tracers (TR-07-17 Intera Engineering Ltd., 20010).   These data will assist in the development of descriptive hydrogeological models of the Bruce DGR site.

7   Acknowledgements

The authors would like to thank R. Thermer for the design and development of the new diffusion cells. Special thanks is extended to W. Müller for the technical support during the experiments.

8   References

Boving, T.B. and P. Grathwohl, 2001. Tracer diffusion coefficients in sedimentary rocks: correlation to porosity and hydraulic conductivity. J. Contam. Hydrol. Vol. 53, pp. 85-100.

Cavé, L., T. Al, Y. Xiang and P. Vilks, 2009. A technique for estimating one-dimensional diffusion coefficients in low-permeability sedimentary rocks using X-ray radiography: comparison with through-diffusion measurements. J. Contam. Hydrol., Vol. 103, pp.1-12.

Crank, J. 1975. The Mathematics of Diffusion. Oxford University Press, second edition, reprinted version, 1998.

Descostes, M., V. Blin, F. Bazer-Bachi, P. Meier, B. Grenut, J. Radwan, M.L. Schlegel, S. Buschaert, D. Coelho, and E.Tevissen, 2008. Diffusion of anionic species in Callovo-Oxfordian argillites and Oxfordian limestones (Meuse/Haute-Marne, France), Appl. Geochem. Vol. 23, pp. 655-677.

Glaus, M.A., W. Müller and L.R. Van Loon, 2008. Diffusion of iodide and iodate through Opalinus Clay: monitoring of the redox state using an anion chromatographic technique. Appl. Geochem. Vol. 23, pp. 3612-3619.

Intera Engineering Ltd., 2010. Technical Report: Measurement of Diffusion Properties by X-Ray Radiography and by Through-Diffusion Techniques Using Iodide and Tritium Tracers: Core Samples from OS-1 and DGR-2, TR-07-17, Revision 3, May 19, Ottawa.

Intera Engineering Ltd., 2009. Project Quality Plan, DGR Site Characterization, Revision 4, August 14, Ottawa.

Intera Engineering Ltd., 2008. Phase 2 Geoscientific Site Characterization Plan, OPG's Deep Geologic Repository for Low and Intermediate Level Waste, Report INTERA 06-219.50-Phase 2 GSCP-R0, OPG 00216-REP-03902-00006-R00, April, Ottawa.

Intera Engineering Ltd, 2007. Test Plan for Measurement of Diffusion Properties by X-Ray Radiography, TP-06-12, Revision 3, October 9, Ottawa. Report prepared by T. Al and L. Cavé, University of New Brunswick.

Intera Engineering Ltd., 2006. Geoscientific Site Characterization Plan, OPG's Deep Geologic Repository for Low and Intermediate Level Waste, Report INTERA 05-220-1, OPG 00216-REP-03902-00002-R00, April, Ottawa.

Ishidera, T. and S. Kurosawa, 2007. Diffusion experiments of HDO and I⁻ with Horonobe sedimentary rocks. Proceedings of the Fall Meeting of the Atomic Energy Society of Japan (AESJ), pp.728-.

Jakob, A., F.A. Sarott and P. Spieler, 1999. Diffusion and sorption on hardened cement pastes – experiments and modeling results. PSI-Bericht Nr. 99-05, Paul Scherrer Institute, Villigen, Switzerland. Also published as NAGRA Technical Report NTB 99-06, Nagra, Wettingen, Switzerland.

Li, Y.-H. and S. Gregory, 1974. Diffusion of ions in sea water and in deep-sea sediments. Geochim. Cosmochim. Acta Vol. 38, pp. 703-714.

Van Loon, L.R., J.M. Soler and M.H. Bradbury, 2003a. Diffusion of HTO, ^{36}Cl⁻ and ^{125}I⁻ in Opalinus Clay samples from Mont Terri: effect of confining pressure. J. Contam. Hydrol. Vol. 61, pp.73-83.

Van Loon, L.R., J.M. Soler, A. Jakob, and M.H. Bradbury, 2003b. Effect of confining pressure on the diffusion of HTO, ^{36}Cl⁻ and 1^{25}I⁻ in a layered argillaceous rock (Opalinus Clay): diffusion perpendicular to the fabric. Appl. Geochem. Vol. 18, pp. 1653-1662.

Van Loon, L.R. and J.M. Soler, 2004. Diffusion of HTO, ^{36}Cl⁻, ^{125}I⁻ and ^{22}Na⁺ in Opalinus Clay: Effect of confining pressure, sample orientation, sample depth and temperature. PSI-Bericht 04-03, Paul Scherrer Institut, Villigen, Switzerland. Also published as Nagra NTB 03-07, Nagra, Wettingen, Switzerland.

Van Loon, L.R., and A. Jakob, 2005. Evidence for a second transport porosity for the diffusion of tritiated water (HTO) in a sedimentary rock (Opalinus Clay – OPA): application of through- and out-diffusion techniques. Transport in Porous Media Vol. 61, pp. 193-214.

Vilks, P. and N.H. Milller, 2007. Evaluation of experimental protocols for characterizing diffusion in sedimentary rocks. Nuclear Waste Management Organization Technical Report TR-2007-11, Toronto.

APPENDIX A

Experimental Data

Experiment: Limestone-1

Sample: DRG2-675.48 (Cobourg Formation)   Filter: Polyethylene

L_{sample}: 7.87 mm L_{filter}: 1.5 mm

$\varnothing_{sample}$: 75.45 mm $\varnothing_{filter}$: 76 mm

W_{sample}: 93.03 g ε_{filter}: 0.45

Dead volume: 3.3 cm^3

C_o: (4.230±0.020)x10^9 Bq m^{-3}

Tracer: ^{125}I$^-$

Glovebox: N_2 (O_2<2ppm)

Time (days)	T (°C)	A_{cum} (Bq)	Error A_{cum} (Bq)	Flux (Bq cm^{-2} d^{-1})	Error Flux (Bq cm^{-2} d^{-1})
0.00	24.8	0	0	0	0
1.99	24.2	30.2	2.1	0.34	0.03
3.99	24.3	175.6	10.5	1.63	0.12
6.99	24.1	499.9	25.6	2.42	0.18
8.99	23.7	751.8	32.1	2.82	0.23
10.99	23.7	1009.9	37.6	2.89	0.23
14.02	24.3	1404.4	47.8	2.91	0.23
16.07	23.5	1679.3	52.1	3.00	0.24
18.08	23.8	1945.2	55.8	2.96	0.23
20.99	24.0	2337.5	62.9	3.02	0.23
22.99	24.0	2612.6	66.2	3.08	0.24
24.99	24.3	2889.3	69.4	3.09	0.24
27.99	25.0	3310.7	76.1	3.14	0.24
29.99	24.0	3592.6	79.0	3.15	0.25
31.99	24.4	3874.2	81.9	3.15	0.25
34.99	24.8	4293.3	87.5	3.12	0.24
36.99	24.7	4581.3	90.2	3.22	0.25
38.99	24.4	4866.3	92.7	3.19	0.25
41.99	24.5	5280.7	97.6	3.09	0.24
43.99	24.3	5578.2	100.4	3.33	0.27
45.99	24.3	5861.6	102.7	3.17	0.25
49.03	24.5	6296.9	107.6	3.20	0.25
51.03	24.4	6579.6	109.8	3.16	0.25
53.03	23.9	6867.8	111.9	3.22	0.25
56.03	24.4	7292.3	116.2	3.17	0.25

Experiment: Limestone-2

Sample: DRG2-675.48 (Cobourg Formation)   Filter: Polyethylene

L_{sample}: 7.69 mm L_{filter}: 1.5 mm

$\varnothing_{sample}$: 75.45 mm $\varnothing_{filter}$: 76 mm

W_{sample}: 90.98 g ε_{filter}: 0.45

Dead volume: 3.3 cm^3

C_o: (4.760±0.054)x10^9 Bq m^{-3}

Tracer: ^{125}I$^-$

Glovebox: N_2 (O_2<2ppm)

Time (days)	T (°C)	A_{cum} (Bq)	Error A_{cum} (Bq)	Flux (Bq cm^{-2} d^{-1})	Error Flux (Bq cm^{-2} d^{-1})
0.00	24.8	0	0	0	0
1.99	24.2	32.4	1.9	0.36	0.03
3.99	24.3	190.4	11.4	1.77	0.13
6.99	24.1	537.4	27.5	2.58	0.19
8.99	23.7	805.9	34.4	3.00	0.24
10.99	23.7	1077.7	40.1	3.04	0.24
14.02	24.3	1493.2	50.7	3.06	0.24
16.07	23.5	1782.1	55.2	3.15	0.25
18.08	23.8	2069.3	59.3	3.19	0.25
20.99	24.0	2489.1	66.9	3.23	0.25
22.99	24.0	2784.8	70.5	3.30	0.26
24.99	24.3	3078.1	73.9	3.28	0.26
27.99	25.0	3526.0	81.0	3.34	0.26
29.99	24.0	3827.9	84.1	3.37	0.27
31.99	24.4	4129.5	87.2	3.37	0.27
34.99	24.8	4579.9	93.3	3.36	0.26
36.99	24.7	4884.6	96.1	3.40	0.27
38.99	24.4	5192.1	98.9	3.44	0.27
41.99	24.5	5636.5	104.2	3.31	0.26
43.99	24.3	5951.7	107.1	3.52	0.29
45.99	24.3	6257.2	109.6	3.41	0.27
49.03	24.5	6722.7	114.9	3.42	0.26
51.03	24.4	7026.5	117.2	3.39	0.27
53.03	23.9	7333.1	119.5	3.43	0.27
56.03	24.4	7792.1	124.2	3.42	0.26

Experiment: Red Shale-1

Sample: DRG2-466-38 (Queenston Formation)   Filter: Polyethylene

L_{sample}: 6.44 mm L_{filter}: 1.5 mm

$\varnothing_{sample}$: 76.01 mm $\varnothing_{filter}$: 76 mm

W_{sample}: 77.21 g ε_{filter}: 0.45

Dead volume: 3.3 cm^3

C_o: (3.991±0.032)x10^9 Bq m^{-3}

Tracer: ^{125}I$^-$

Glovebox: N$_2$ (O$_2$<2ppm)

Time (days)	T (°C)	A_{cum} (Bq)	Error A_{cum} (Bq)	Flux (Bq cm^{-2} d^{-1})	Error Flux (Bq cm^{-2} d^{-1})
0.00	25.0	0	0	0	0
0.99	24.4	29.2	2.054	0.65	0.05
1.99	24.0	340.9	22.059	6.87	0.51
3.99	24.4	1584.8	90.989	13.71	1.02
6.99	24.8	3922.9	191.656	17.17	1.30
8.99	24.7	5669.9	233.853	19.25	1.54
10.99	24.4	7401.0	267.863	19.07	1.50
13.99	24.5	9893.5	324.352	18.31	1.40
15.99	24.3	11681.9	352.681	19.71	1.59
17.99	24.3	13433.3	376.998	19.29	1.53
21.03	24.5	16094.8	424.964	19.29	1.49
23.03	24.4	17832.1	444.829	19.14	1.51
25.03	23.9	19601.7	464.196	19.50	1.53
28.03	24.4	22232.5	503.043	19.33	1.49
30.03	24.4	23970.4	519.941	19.21	1.52
32.03	24.3	25739.2	536.579	19.43	1.52
35.03	24.4	28415.3	571.596	19.66	1.51
37.03	23.4	30201.1	587.164	19.68	1.54
39.03	24.3	31993.4	602.353	19.75	1.55
42.03	24.4	34644.3	633.417	19.47	1.50

Experiment: Red Shale-1

Sample: DRG2-466-38 (Queenston Formation)   Filter: Polyethylene

L_{sample}: 9.08 mm L_{filter}: 1.5 mm

$\varnothing_{sample}$: 76.01 mm $\varnothing_{filter}$: 76 mm

W_{sample}: 109.24 g ε_{filter}: 0.45

Dead volume: 3.3 cm^3

C_o: $(3.974\pm0.038)\times10^9$ Bq m^{-3}

Tracer: $^{125}I^-$

Glovebox: N$_2$ (O$_2$<2ppm)

Time (days)	T (°C)	A_{cum} (Bq)	Error A_{cum} (Bq)	Flux (Bq cm^{-2} d^{-1})	Error Flux (Bq cm^{-2} d^{-1})
0.00	24.4	0.0	0	0	0
1.00	23.8	0.9	0.1	0.02	0.00
2.00	23.4	29.4	2.0	0.63	0.05
4.00	24.3	352.4	22.8	3.56	0.26
7.00	24.4	1363.8	75.6	7.43	0.56
9.00	23.2	2257.7	101.1	9.85	0.77
11.00	23.2	3209.3	123.6	10.49	0.82
14.00	23.5	4711.5	165.8	11.03	0.85
16.00	23.2	5732.4	182.7	11.25	0.88
18.00	23.6	6767.0	198.6	11.40	0.90
21.00	23.3	8338.8	229.9	11.55	0.89
23.00	23.3	9377.2	242.8	11.44	0.90
25.00	23.3	10436.0	255.5	11.67	0.91
28.00	22.8	12018.4	281.0	11.62	0.90
30.00	22.6	13071.8	291.9	11.61	0.91
32.00	23.1	14127.0	302.5	11.63	0.91
35.00	23.0	15714.3	324.5	11.66	0.90
37.00	23.7	16790.5	334.4	11.86	0.93
39.00	23.7	17870.9	344.1	11.90	0.93
42.00	24.1	19505.2	364.5	12.01	0.92